Performance analysis and PCM selection for adsorption chiller aided by energy storage supplied from the district heating system

JAROSŁAW KARWACKI[a*]
ROMAN KWIDZINSKI[a]
PIOTR LEPUTA[a,b]

[a] The Szewalski Institute of Fluid Flow Machinery, Polish Academy of Sciences, Heat Transfer Department, Fiszera 14, 80-231 Gdańsk, Poland

[b] ENERGA Ciepło Ostrołęka Sp. z o.o., Celna 13, 07-410 Ostrołęka, Poland

Abstract   The paper presents a theoretical analysis of thermal energy storage filled with phase change material (PCM) that is aimed at optimization of an adsorption chiller performance in an air-conditioning system. The equations describing a lumped parameter model were used to analyze internal heat transfer in the cooling installation. Those equations result from the energy balances of the chiller, PCM thermal storage unit and heat load. The influence of the control of the heat transfer fluid flow rate and heat capacity of the system components on the whole system operation was investigated. The model was used to validate the selection of Rubitherm RT62HC as a PCM for thermal storage. It also allowed us to assess the temperature levels that are likely to appear during the operation of the system before it will be constructed.

Keywords: Thermal sorption cooling; Phase change material; Thermal energy storage; District heating; Adsorption; Energy management; Mathematical modelling; Load shifting, Efficiency

*Corresponding Author. Email: jkarwacki@imp.gda.pl

Nomenclature

A	–	heat transfer area, m^2
c	–	specific heat, J/kgK
E	–	thermal energy, J, kWh
h_p	–	partial enthalpy, J/kg
k	–	overall heat transfer coefficient, W/m^2K
l	–	length, m
$\dot{m}$	–	mass flow rate, kg/s
M	–	mass, kg
P	–	electric power, W
Q	–	heat flow rate, W
R	–	thermal resistance, K/W
T	–	temperature, °C
x	–	3-way valve setting

Greek symbols

α	–	heat transfer coefficient, W/m^2K
δ	–	heat conduction thickness, m
λ	–	thermal conductivity, W/(m·K)
τ	–	time, s, h

Subscripts

a	–	surroundings
b	–	non-conditioned air
c	–	PCM heat storage
d	–	district heating network
e	–	evaporation
f	–	floor
g	–	adsorption chiller heat generator loop
h	–	air cooler
i	–	indoor air
in	–	insulation
m	–	modelled parameter
o	–	window
p	–	inner wall
s	–	heat sources in office room (solar irradiation, people, computers, etc.)
u	–	ceiling
v	–	solar heat storage
w	–	outer wall

Abbreviations

AC	–	air conditioning
HTF	–	heat transfer fluid
LHTES	–	latent heat thermal energy storage
PCM	–	phase change material
TES	–	thermal energy storage

1   Introduction

Climate changes, progressive thermal modernization of buildings, and changes in the habits of their users cause that local heat sources (local gas boiler plants) have become heavily oversized. This problem also concerns extensive district heating network systems. The above circumstances result in undertaking a variety of actions, including research. The most important of them are attempts to increase the flexibility of power generation units (coal, biomass, gas fired), searching for new energy sources with a reduced impact on the environment (e.g. geothermal sources, biogas, heat pumps), as well as activities on the optimization of existing systems while minimizing the degree of interference in their structure. One of the methods used in the optimization is energy storage in periods of overproduction to use the stored energy in periods of increased demand. Currently, the commonly used technology is the accumulation of sensible heat in hot water tanks. This applies both to large-scale facilities [1, 2], and solutions used by end users in heat substations of individual buildings [3, 4]. In many cases, the size of such tanks is a significant disadvantage that causes implementation difficulties, particularly in existing networks, which are usually distributed over an urban structure. For this reason, this work deals with the subject of developing a dedicated latent heat thermal energy storage (LHTES), suitable to operate in a modern district heating network. The target area of application of this type of storage are district heating networks, primarily in European countries but also in other areas.

There are over 440 district heating systems in Poland and the installed thermal capacity is 53.3 GW [5]. The total length of heating networks in Poland increased between 2015 and 2020 by approx. 8% with an increase in ordered capacity by approx. 3.4% [5,6], which may indicate a stable development of existing heating systems. In Poland, 53% of citizens use district heat [6]. In the heating systems, about 8.6% of the installed capacity comes from gas sources [7, 8], which have the highest percentage share among boilers up to 5 MW, amounting to 37%. This significant number of heating sources constitutes the primary market in which the proposed storage can be applied. The use of LHTES can significantly reduce the consumption of primary fuels by these heating installations. According to Euroheat and Power (2015) 57% of customers in Lithuania use district heating, 24% in Austria, 65% in Latvia, and 35% in Slovakia. These few examples show the enormous scale of possible expansion, especially when it will be taken into account that small boiler houses constitute a large group in many of the

mentioned countries, next to the country's dominant high-power coal-fired power plants. Savings achieved through the use of the developed storage, due to the possible scale of application, can noticeably reduce the consumption of primary fuels. It should be mentioned here that the savings gained from the already existing sources, resulting from the increase of their efficiency, are the cheapest and the most effective method of reducing emissions and limiting the consumption of primary fuels. There are also proposals for operational optimization of district heating systems by using thermal inertia of the network [9].

Another challenge facing the district heating sector is the need to introduce new technologies in order to provide customers with a new type of services. There is more and more talk about the need to use heat from the existing district heating network to generate cold, e.g. by adsorption chiller. Unfortunately, there is often a case in which the typical infrastructure of a heating network does not allow the proper supply of the chiller at the end user substation. Too low mass flow and/or periodically too low feeding temperature in the supply line causes the adsorption unit to operate with a reduced cooling capacity. The use of the LHTES will enable the adsorption unit to work around the clock. The energy accumulated at night in the LHTES will allow us to cover the cooling demand in the peak hours. It will also reduce dependence on technical constraints related to the existing heat supply infrastructure. In addition, such a solution will have a positive effect on the entire heating network due to the reduction of the return water temperature at the heat and power plant. Summing up, the widespread implementation of the LHTES units can significantly reduce losses in heating systems. The problems of LHTES optimal operation and integration with heating systems are discussed, e.g. in [2,10,11].

Thermally driven absorption, adsorption and ejection cooling systems are known and used for many years [12]. Nowadays such systems become more and more popular, especially where opportunities exist for trigeneration and applications utilizing waste heat [13, 14]. For example, hybrid solar-gas driven and air-cooled absorption chiller integrated with hot water production was evaluated theoretically by Rad and Davoodi [15]. Their analysis focused on energetic, exergetic and economic aspects to find the optimum generator temperature in the LiBr absorption chiller and natural gas consumption. Rouf *et al.* [16] studied the performance of a solar heat driven adsorption chiller with a new parallel system of 4 beds. It was concluded that the cooling capacity of the proposed 4-bed chiller can be improved, especially when the heat source power is limited. This results from

a better distribution of the adsorbent in multiple beds and the lengthened pre-cooling time. Naseem *et al.* [17] published experimental results and theoretical analysis of a trigeneration system consisting of an adsorption chiller driven by waste heat from a high temperature proton exchange membrane fuel cell.

The main focus of the present research is the integration of a cooling system with the adsorption chiller driven by district heat [18–20]. Similar concepts are reported in the literature as the next (5th) generation of district heating systems [20, 21]. In summer, district heating systems struggle with a problem of low profitability due to limited heat consumption. Integration of the heat-driven chilling units with district heating systems will be a step to resolve this issue. The adsorption chillers seem to be a perspective technology in district heating systems. However, their development is limited by the temperature of the heat source which may be too low to ensure their efficient operation. This study concerns a real industrial case in which there is a mismatch between the heating system and the adsorption chiller operating in an office building's air conditioning (AC) system (Fig. 1). In this application, the heat flow rate from available motive hot water was too low to properly supply the adsorption chiller during peak load periods. Therefore, a thermal energy storage system with a phase change material (PCM) was suggested to reduce the peak cooling load demand.
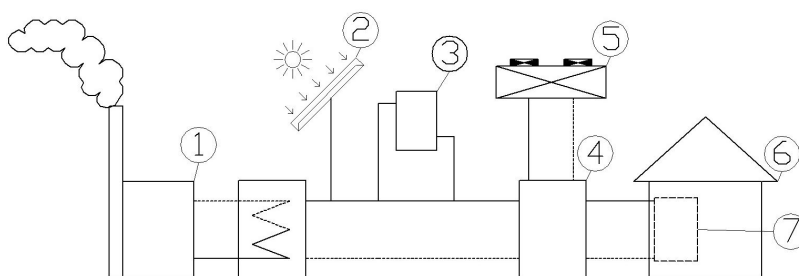

Figure 1: General scheme of the cooling system: 1 – district heating system, 2 – solar heating system, 3 – thermal energy storage, 4 – adsorption chiller, 5 – recooling system, 6 – office building, 7 – air cooler.

Currently, phase change materials (PCMs) are used both in low- and high-temperature applications [23–25]. PCM heat storage systems utilize the process of phase change between solid and liquid to store thermal energy. The heat transfer process during melting and solidifying proceeds at a nearly constant temperature. In a narrow range around the phase

change temperature, the PCM stores and releases large quantities of thermal energy [26]. In cooling applications, water is the most popular PCM. Ice banks with a chiller are used in cooling and air conditioning systems for storing thermal energy produced during off-peak periods to meet the thermal load that occurs during high-demand periods. They work during nighttime, when the energy costs are low, and use the accumulated cooling energy during day time. Ice bank systems allow for using a cooling aggregate with a much smaller cooling power than the peak cooling load appearing during the AC system's operation. Thermal comfort inside the building may also be improved in a passive way by PCM implanted directly in the building structure, i.e walls, ceilings [27, 28].

A review of the PCMs' use in solar absorption refrigeration systems was prepared by Khan *et al.* [29]. It discusses LHTES technologies, the selection of suitable PCM, methodologies of integration, enhancement techniques, cost analyses and challenges related to PCM usage in refrigeration systems. Recent, more general reviews of sorption refrigeration driven by low-grade heat sources can be found in the papers by Almasri *et al.* [30], Chauhan *et al.* [31], Hassan *et al.* [32], and Ullah *et al.* [33].

Using PCM to store the cooling energy produced by a photovoltaic-driven vapor compression chiller was proposed by Varvagiannis *et al.* [34]. They propose a novel refrigerant-PCM-water heat exchanger to replace the evaporator of the conventional chiller. Based on the semi-dynamic modelling of the considered system, it is concluded that the proposed hybrid storage system shows improved performance, limiting the cooling demand peaks and enhancing the fraction of solar energy in cooling production, especially for partial cooling loads. Ghorbani *et al.* [35] modelled and optimized solar-charged latent heat storage to power a single effect LiBr/water absorption chiller. In this way, the cooling and heating demand of a building can be met during the absence of enough sunlight. The storage unit thermal response was modelled numerically and its geometry was optimized using a multi-objective genetic algorithm to simultaneously minimize the charging and maximize the discharging time. Numerical studies concerning the design of LHTS units with different fin configurations and selection of a proper PCM for solar adsorption cooling systems were performed by Raj *et al.* [36]. Due to the complexity of the interaction between all elements of the heating/cooling system, a theoretical estimation of the LHTS profits is hard to perform in a reliable way. In order to solve this problem, the application of energy storage filled with PCM was experimentally investigated by Karwacki [37]. A case study of an actual adsorption cooling plant with

different fin shapes in the LHTS showed that the optimum fin configuration can save up to 46% of the heat storage cost as compared to LHTES without fins. One of the most efficient heat transfer enhancement methods found in modern exchangers is based on the use of microlamellas or microchannels or highly developed heat transfer surfaces in the form of perforated plates with microholes or porous materials [39,40]. This method, originating from the field of "large scale" thermoaerodynamics [41, 42], is still a challenge in terms of application for heat exchangers. Some of the reasons for this are due to the different geometries and the problems with optical access, making it very difficult to use the methods that are widely available in the before mentioned field of thermodynamics [43] that give a good insight into the temperature field.

2   Materials and methods

2.1   System description

The studied heat transfer system uses low-grade heat from district heating to produce chilled water for air conditioning in an office building. A simplified schematic of the system arrangement is shown in Fig. 2.
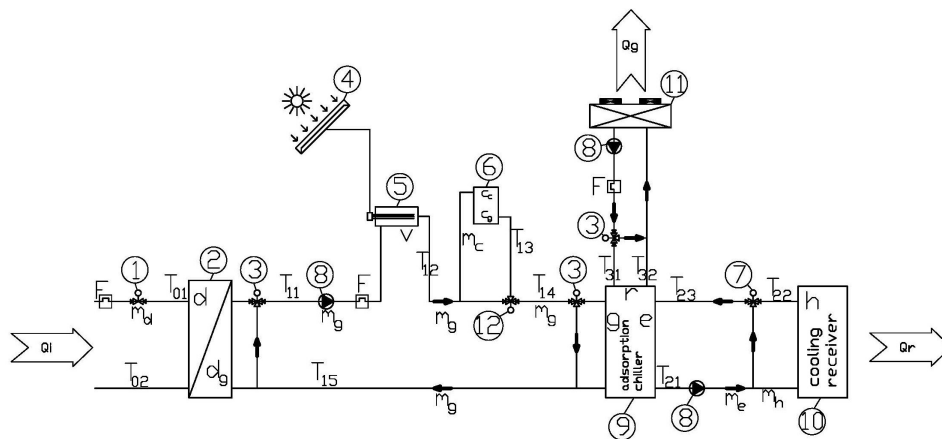
Figure 2: The scheme of the cooling system configuration: 1 – regulating valve, 2 – district heating heat exchanger, 3 – 3-way on/off valve, 4 – photovoltaic panels, 5 – electric heater, 6 – LHTES, 7 – 3-way mixing valve in cooling circuit, 8 – circulating pump, 9 – adsorption chiller, 10 – office building, 11 – drycooler, 12 – 3-way mixing valve in driving (hot) circuit, F – flowmeter, T – temperature. Lowercase letters indicate elements included in model equations.

The proposed cooling system was designed to provide AC for the office building located in Ostrołęka (Poland) in which 7 rooms will be cooled. The plan view of the office is shown in Fig. 3 and its dimensional and thermal parameters are collected in Table 1. The cooling load of the conditioned rooms originates from the heat transferred from three sources: the environment, workers and electric appliances (essentially personal computers).
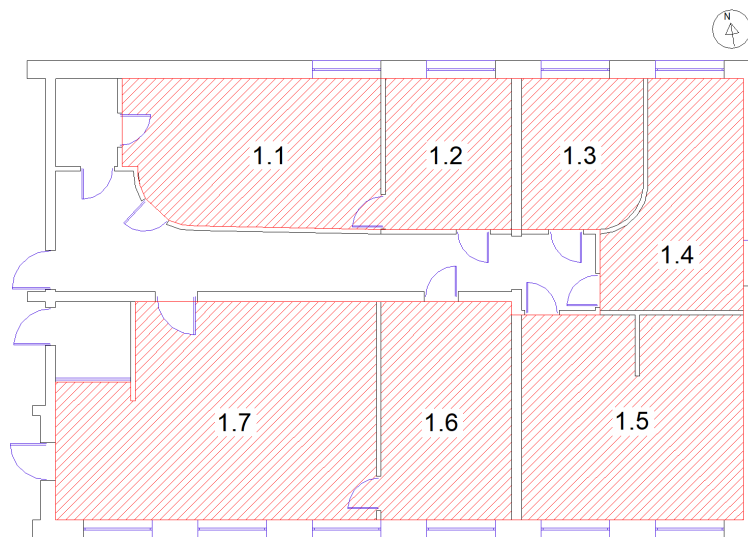

Figure 3: The schematic view of the office building.

Table 1: Office rooms data.

Room No.	Cardinal direction	Ext. wall length (m)	Windows area (m²)	Walls area (m²)	Room volume (m³)	Wall thickness (m)	Wall heat conductivity (W/m·K)	Wall specific heat (J/kgK)	Wall density (kg/m³)	Number of workers
1.1	North	6.72	7.2	13.96	75.66	0.44	0.37	900	1488	–
1.2	North	3.36	3.6	6.48	38.02	0.44	0.37	900	1488	1
1.3	North	3.36	3.6	6.48	37.51	0.44	0.37	900	1488	1
1.4	East	6.36	2.4	16.67	64.95	0.44	0.37	900	1488	2
	North	2.96	3.6	5.28		0.44	0.37	900	1488	
1.5	South	6.44	7.2	12.12	97.57	0.44	0.37	900	1488	3
	East	5.68	0.0	17.05		0.44	0.37	900	1488	
1.6	South	3.27	3.6	6.21	49.54	0.44	0.37	900	1488	2
1.7	South	8.76	10.8	15.48	132.63	0.44	0.37	900	1488	4

Based on historical data for the office building, the ambient temperature and the supply parameters of the central heating exchanger were determined. The air temperature was measured from January 1st to December 31st, 2020, by the weather station Lufft WS700-UMB installed at the building. The time history of these parameters is shown in Figs. 4, 5 and 6.
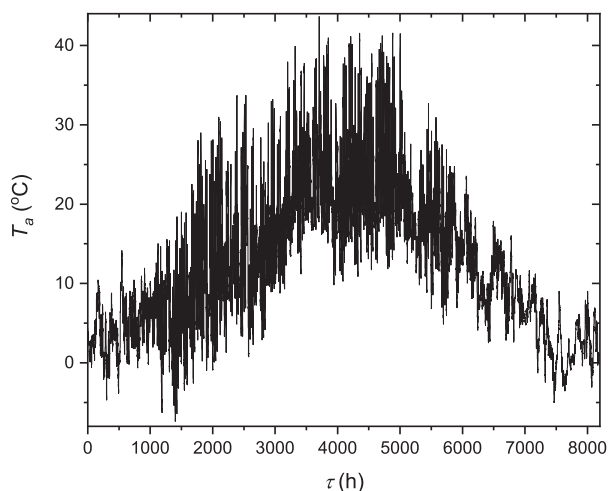

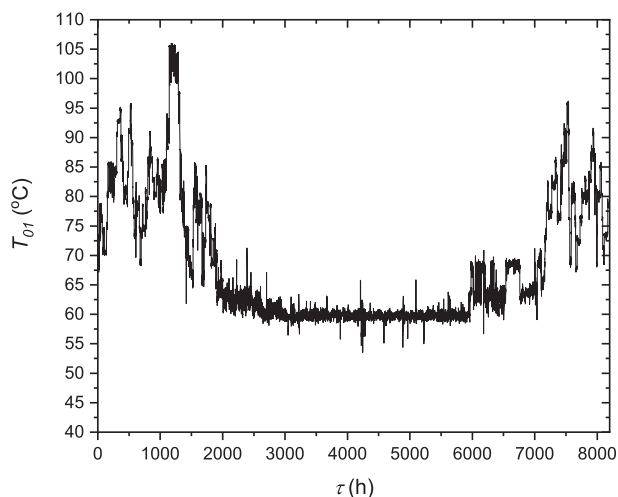Figure 4: Ambient air temperature from January 1st to December 31st, 2020.

Figure 5: District heating water supply temperature at the substation exchanger inlet from January 1st to December 31st, 2020.
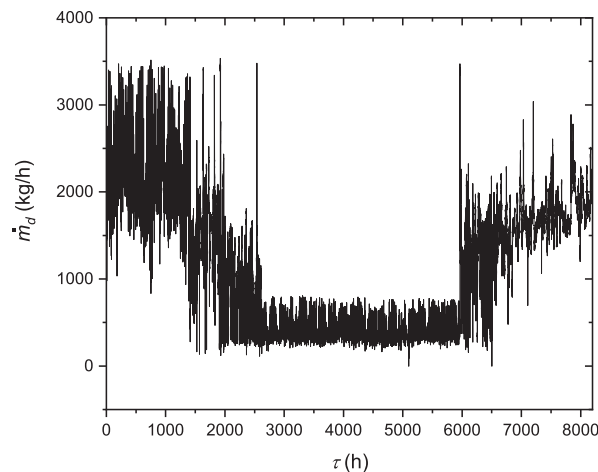
Figure 6: Mass flow rate of the district heating water supply at the substation exchanger inlet from January 1st to December 31st, 2020.

The following studies were carried out to prepare input data for simulation tests:

- variants of the heat storage operation were determined,

- representative daily profiles of the input parameters were selected,

- cooling load from the office building was determined,

- heat transfer characteristics of the substation exchanger were determined,

- adsorption chiller meeting the system requirements was selected.

It has been assumed that the cooling system will maintain the temperature of 25°C in the rooms and will operate from 7 a.m. to 4 p.m.

After examining the all-year ambient temperature profile (see Fig. 4), one daily profile recorded on July 22, 2020 was selected. This was one of the days with the highest average temperature of the year at the office location. The selected hourly ambient temperature profile is presented in Fig. 7. The resolution of the ambient temperature recordings is 15 min. During the selected day, the lowest ambient temperature of 18°C was recorded shortly before sunrise. During the daytime, it rose to a maximum of 31°C. The corresponding profiles of supply temperature and mass flow rate in

the district heating substation exchanger on July 22, 2020 are shown in Figs. 8 and 9. The supply water temperature was highest during the night, with a maximum value of 62°C, and slightly dropped during the daytime to 60°C. The mass flow rate decreased significantly during the day. If an adsorption chiller is used to power the air conditioning, this circumstance will cause a drastic decrease in cooling capacity. The application of heat storage should in this case significantly support the refrigeration system.
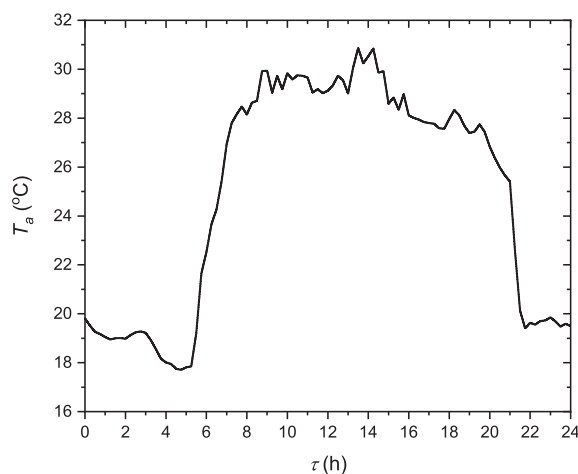

Figure 7: Daily ambient temperature profile on July 22, 2020.
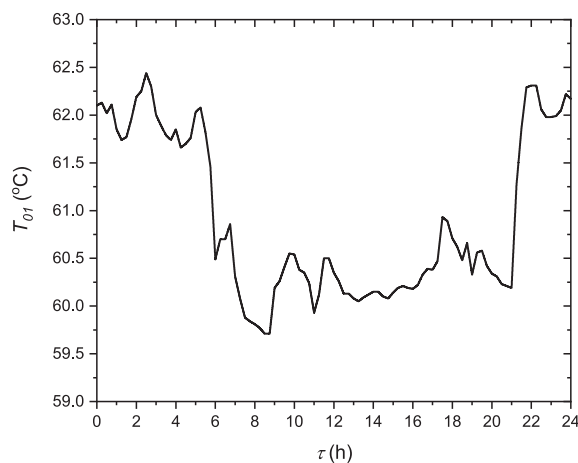
Figure 8: Daily temperature profile of the district heating water supply at the substation exchanger inlet on July 22, 2020.
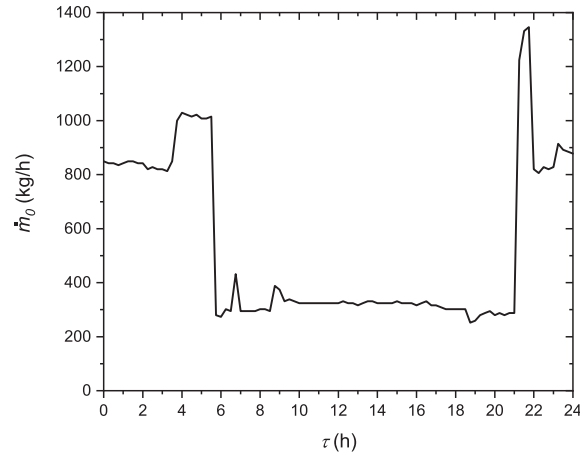
Figure 9: Daily mass flow rate profile of the district heating water supply at the substation exchanger on July 22, 2020.

To determine the total cooling load due to internal heat sources in the office, it was assumed that the average heat gain from a person is 70 W. The number of persons in each office room is listed in Table 1. Not all of them are present in their rooms throughout the working day so it was assumed that the average occupancy factor is 0.75. The heat generated by electrical appliances was estimated to be constant and equal to 3 kW in total. Radiation was taken into account for the heat transferred from the ambient through the sunlit walls and windows in a way described in [20].

In the calculations of the hot water supply, the parameters of a JAD 6.5 type heat exchanger manufactured by Secespol were adopted for the substation. This heat exchanger was used so far in the building for the central heating installation. Because the cooling system will be used only in a part of the building, 1/4 of the heat transfer surface of the exchanger was taken for the calculations. This corresponds to the assumption that the cooling system will be installed without interfering with the substation circulation from the district network side.

The data presented above allow us to determine the working parameters of the chiller unit eCoo 2.0 manufactured by SorTech AG (currently Fahrenheit GmbH) [44]. The requirements of the investigated AC system are met by the chiller of refrigeration power up to 16 kW and maximum coefficient of performance (COP) of 0.65. It operates with the hot water temperature 50–95°C and recooling temperature 22–40°C, producing chilled water of 8–21°C. Nominal flow rates are 2.5 m^3/h in the hot water circuit, 5.1 m^3/h in

recooling and 2.9 m^3/h of chilled water. Characteristics of cooling capacity as functions of hot, recooling and chilled water temperatures were provided by the manufacturer. These data were used to prepare own characteristics in the form of a continuous interpolated function that was required in the chiller simulations.

The analysis of the temperature distributions shows that during the period of the highest ambient temperatures (Fig. 7), and thus the greatest demand for cooling of the office spaces, the supply temperature ranges from 59°C to 62°C. It is a low value in relation to the nominal operating parameters of the adsorption chiller. Moreover, it should be taken into account that on the supply side of the chiller, in the high temperature circuit, the temperature will be even lower. Estimating this value, as indicated above, is difficult due to the interdependence between the various components of the system. This estimation, however, is necessary for the selection of the PCM. Also, both the cooling capacity of the chiller and the overall cooling demand of the office depend on the ambient temperature. Therefore, more accurate predictions of the system performance will be carried out using the equations of the lumped-parameter model described in Section 3.

2.2   Phase change material selection

The knowledge of thermophysical properties of heat storage materials is essential in LHTES design and operation. Due to the differences in physical, chemical, thermal and functional properties, the selection procedure of a PCM for LHTES should take into account many criteria and allow us to find the most optimum material composition. Considering the PCM, knowledge of the specific heat for both the liquid and solid states is necessary as well as the phase transition temperature and specific heat of fusion. These parameters are often determined using the well-known differential scanning calorimetry (DSC) technique [45, 46] or the T-history method [47]. Based on the known thermophysical properties, it is possible to estimate the thermal capacity of the storage but this only applies to the quasi steady-state conditions. As the research reported in [48] shows, the results obtained for a storage in which the PCM is subjected to dynamic temperature inputs, deviate from the theoretical predictions. Therefore, in this work, mathematical modelling was used to support the PCM selection process. When selecting the PCM, it was assumed that the heat transfer fluid (HTF) inlet temperature from the district heating will be in the range of 55–90°C. This means that the PCM phase transition temperature should also be within

these limits. Therefore, initially six commercially sold PCMs were considered: ATP 60, ATP 70, Croda Therm 60, RT62HC, RT69HC and RT70HC. Well-documented parameters, cycling stability and low supercooling were the reasons for choosing these PCMs. The partial enthalpy distributions for these materials, based on manufacturer data, are presented in Figs. 10–15.
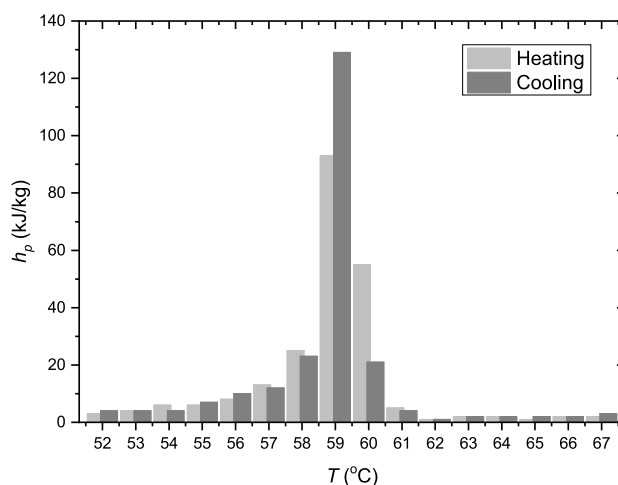
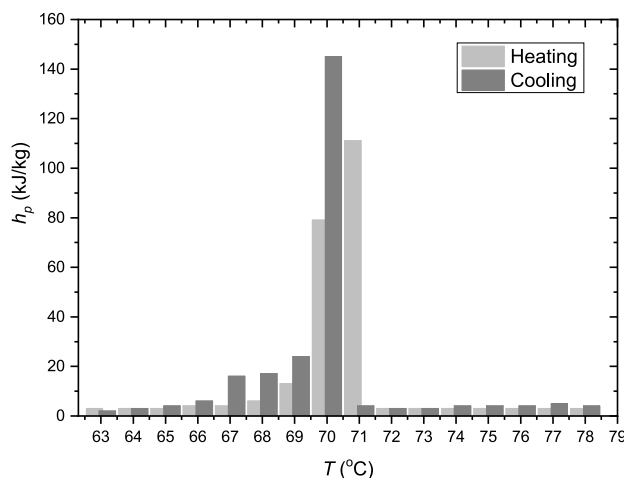Figure 10: Partial enthalpy distribution as a function of temperature during heating and cooling for the phase change material Axiotherm ATP 60 [49].

Figure 11: Partial enthalpy distribution as a function of temperature during heating and cooling for the phase change material Axiotherm ATP 70 [50].
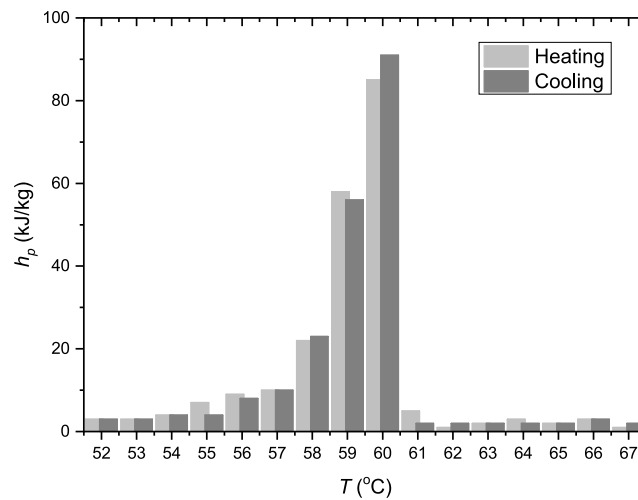
Figure 12: Partial enthalpy distribution as a function of temperature during heating and cooling for the phase change material Croda Therm 60 [51].
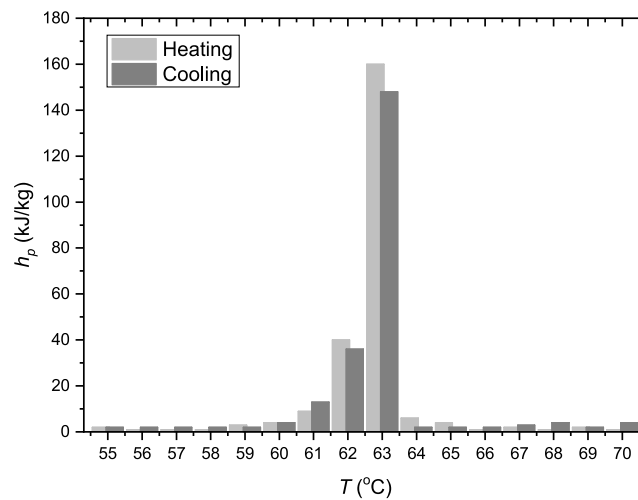

Figure 13: Partial enthalpy distribution as a function of temperature during heating and cooling for the phase change material Rubitherm RT62HC [52].

Most of the pre-selected PCMs require a supply temperature of the district heating substation above 70°C. During the period of demand for air conditioning, such conditions occur in the transitional seasons, i.e. in spring and autumn. During the peak air conditioning demand (in summer), sup-
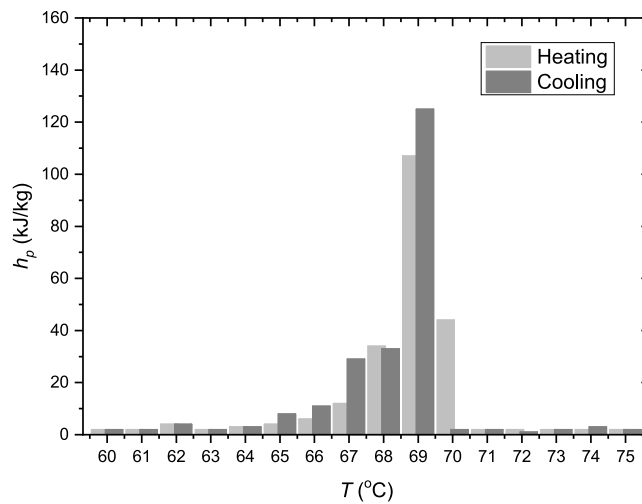
Figure 14: Partial enthalpy distribution as a function of temperature during heating and cooling for the phase change material Rubitherm RT69HC [53].
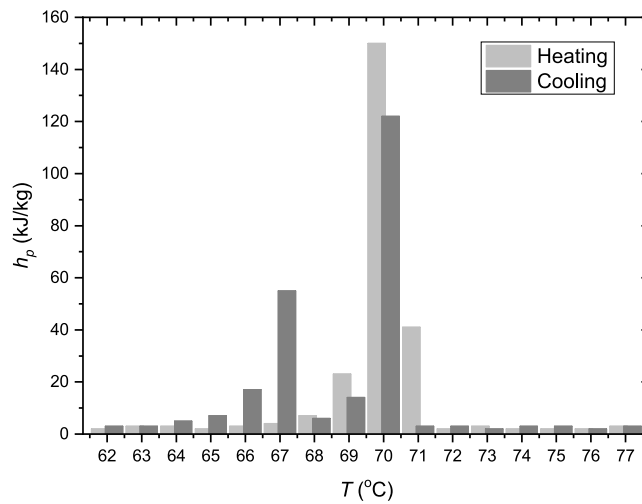

Figure 15: Partial enthalpy distribution as a function of temperature during heating and cooling for the phase change material Rubitherm RT70HC [54].

ply temperatures are around 62°C as seen in Fig. 5. For this reason, the RT62HC material was selected for further analysis. A summary of its primary thermophysical properties is presented in Table 2.

Table 2: Summary of the primary thermophysical properties of Rubitherm RT62HC.

Parameter	Value
Melting area	62–63°C
Congealing area	62°C
Heat storage capacity (latent and sensible heat)	230 kJ/kg
Specific heat capacity (both phases)	2 kJ/kgK
Solid density (at 20°C)	0.85 kg/l
Liquid density (at 80°C)	0.84 kg/l
Heat conductivity (both phases)	0.2 W/mK

3 Computational model of the cooling system and office building

Thermal dynamics of the cooling system consisting of the adsorption chiller, cold receiver (office building), thermal energy storage and control valves was analyzed by means of a 0D lumped-parameter mathematical model based on the heat balance equations. The solution of model equations can be used to validate the selection of PCM for thermal storage. It also allows us to assess and track temperature levels that are likely to appear during the system operation. Furthermore, it can be used as a tool in the design of the system control loop.

In the model, the heat capacities of the liquid loop and all the above mentioned system elements were taken into account. For simplicity, it was assumed that heat transfer occurs by conduction and convection only. Thermal radiation is not considered, except for solar irradiation which is included in calculations of the air temperature inside the office. The equations of the model are based on a balance between the rate of heat flow accumulated in the material of a mass M and specific heat c, and the difference of the supplied ($\dot{Q}_{in}$) and dissipated ($\dot{Q}_{out}$) heat flow rates. This balance can be written in the following general form:

$$\dot{Q} = Mc\frac{dT}{d\tau} = \sum \dot{Q}_{in} - \sum \dot{Q}_{out}(\tau), \qquad (1)$$

where τ denotes time.

3.1   Office building

It was assumed that the analyzed room space of the building is located between two identical floors. This means that the temperatures on both sides of the horizontal partition (ceiling/floor) are the same. Figure 3 shows the schematic view of the office level. Figure 16 shows the building elements included in the mathematical model. Detailed information about the items is provided in Table 3.
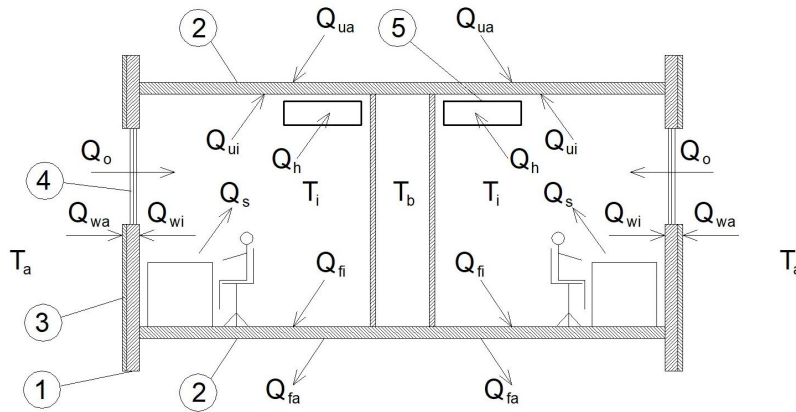

Figure 16: The schematic view of the model office building: 1 – outer wall, 2 – ceiling/floor, 3 – insulation, 4 – window, 5 – air cooler.

Table 3: OfDetailed information about the elements included in the office model.

Parameter	A (m^2)	ρ (kg/m^3)	M (kg)	c (J/kgK)	λ (W/m K)	α (W/m^{2}K)	k (W/m^{2}K)
Outer wall (w)	85.8	800.0	56155	800	0.33	–	–
Inner wall (p)	96.4	–	20392	800	–	–	–
Ceiling (u)	142.1	2300.0	49453	800	0.09	–	–
Floor (f)	142.1	2300.0	58240	800	0.08	–	–
Windows (o)	34.8	–	–	–	–	–	1.1
Indoor air (i)	–	1.2	–	1000	–	5	–
Ambient air (a)	–	1.2	–	1000	–	10	–
HTF (h)	–	1000.0	40	4200	–	–	6.0

The proposed simplified numerical model of the office building describes heat transfer and accumulation between the indoor air and the wall, as

well as the heat transfer to or from the surroundings. The model presented is similar to the one presented in [37, 55]. Based on Eq. (1), the balance equations for each material accumulating heat in the building can be written as follows:

indoor air

$$M_i c_i \frac{dT_i}{d\tau} = \dot{Q}_h + \dot{Q}_{wi} + \dot{Q}_{pi} + \dot{Q}_{fi} + \dot{Q}_{ui} + \dot{Q}_o + \dot{Q}_s \,, \tag{2}$$

or

$$
\begin{aligned}
M_i c_i \frac{dT_i}{d\tau} = {} & \frac{(T_h - T_i)}{R_h} + \frac{(T_w - T_i)}{R_{wi}} + \frac{(T_p - T_i)}{R_{pi}} \\
& + \frac{(T_f - T_i)}{R_{fi}} + \frac{(T_u - T_i)}{R_{ui}} + \frac{(T_a - T_i)}{R_o} + \dot{Q}_s \,,
\end{aligned} \tag{3}
$$

where the right hand side terms represent heat flow rates from the air cooler $(\dot{Q}_h)$, people, solar irradiation and other heat sources $(\dot{Q}_s)$ as well as heat transferred through the walls $(\dot{Q}_{wi}, \dot{Q}_{pi})$, floor $(\dot{Q}_{fi})$, ceiling $(\dot{Q}_{ui})$, and windows $(\dot{Q}_o)$;

HTF in air cooler

$$M_h c_h \frac{dT_h}{d\tau} = \dot{m}_h c_h (T_{21} - T_{23}) + \frac{T_i - T_h}{R_h} \,, \tag{4}$$

where

$$T_h = \frac{(T_{21} + T_{23})}{2} \,; \tag{5}$$

and T_{21}, T_{23} are evaporator and cooler outlet temperatures, respectively;

outer wall

$$M_w c_w \frac{dT_w}{d\tau} = -\dot{Q}_{wi} + \dot{Q}_{wa} = \frac{T_i - T_w}{R_{wi}} + \frac{T_a - T_w}{R_{wa}} \,; \tag{6}$$

inner wall

$$M_p c_p \frac{dT_p}{d\tau} = -\dot{Q}_{pi} + \dot{Q}_{pb} = \frac{T_i - T_p}{R_{pi}} + \frac{T_{pb} - T_p}{R_{pb}} \,; \tag{7}$$

floor

$$M_f c_f \frac{dT_f}{d\tau} = -\dot{Q}_{fi} + \dot{Q}_{fa} = \frac{T_i - T_f}{R_{fi}} + \frac{T_{fa} - T_f}{R_{fa}} \,; \tag{8}$$

ceiling

$$M_u c_u \frac{dT_u}{d\tau} = -\dot{Q}_{ui} + \dot{Q}_{ua} = \frac{T_i - T_u}{R_{ui}} + \frac{T_{ua} - T_u}{R_{ua}} \,. \tag{9}$$

In the above equations, heat transfer from the liquid zones and surroundings was treated as purely convective. In the remaining zones, only conductive heat transfer was assumed. The thermal resistance between the individual heat exchange surfaces can be written as:

outer wall – indoor air

$$R_{wi} = \frac{1}{A_w} \left(\frac{1}{\alpha_{wi}} + \frac{\delta_w}{2\lambda_w} \right); \tag{10}$$

outer wall – ambient air

$$R_{wa} = \frac{1}{A_w} \left(\frac{1}{\alpha_{wa}} + \frac{\delta_w}{2\lambda_w} \right); \tag{11}$$

inner wall – indoor air

$$R_{pi} = \frac{1}{A_p} \left(\frac{1}{\alpha_{pi}} + \frac{\delta_p}{2\lambda_p} \right); \tag{12}$$

inner wall – non-conditioned air

$$R_{pb} = \frac{1}{A_p} \left(\frac{1}{\alpha_{pb}} + \frac{\delta_p}{2\lambda_p} \right); \tag{13}$$

floor – indoor air

$$R_{fi} = \frac{1}{A_f} \left(\frac{1}{\alpha_{fi}} + \frac{\delta_f}{2\lambda_f} \right); \tag{14}$$

floor – non-conditioned air

$$R_{fa} = \frac{1}{A_f} \left(\frac{1}{\alpha_{fa}} + \frac{\delta_f}{2\lambda_f} \right); \tag{15}$$

ceiling – indoor air

$$R_{ui} = \frac{1}{A_u} \left(\frac{1}{\alpha_{ui}} + \frac{\delta_u}{2\lambda_u} \right); \tag{16}$$

ceiling – non-conditioned air

$$R_{ua} = \frac{1}{A_u} \left(\frac{1}{\alpha_{ua}} + \frac{\delta_u}{2\lambda_u} \right); \tag{17}$$

air cooler – indoor air

$$R_h = \frac{1}{k_h A_h}, \tag{18}$$

window – indoor air

$$R_o = \frac{1}{k_o A_o}. \tag{19}$$

3.2   Phase change material heat storage

The phase change material heat storage is described in terms of the lumped-parameter model. Using the notation explained in Fig. 2, the following heat balance equations may be written:

PCM in LHTES3:

$$M_c c_c(T_c) \frac{dT_c}{d\tau} = \frac{T_{cg} - T_c}{R_{cg}} - \dot{Q}_{ca} \,, \tag{20}$$

HTF in LHTES3:

$$M_{cg} c_g \frac{dT_{cg}}{d\tau} = \dot{m}_c c_g \left(T_{12} - T_{13}\right) + \frac{T_c - T_{cg}}{R_{cg}} \,, \tag{21}$$

where

$$T_{cg} = \frac{T_{12} + T_{13}}{2} \,, \tag{22}$$

$\dot{Q}_{ca}$ is the rate of heat flow to the surroundings and T_{12}, T_{13} are temperatures at the LHTES3 inlet and outlet, respectively.

3.3   Adsorption chiller

The set of lumped-parameter model equations is completed with formulas describing the adsorption chiller and its connections with the office air cooler, PCM storage, electrically heated water tank and district substation heat exchanger, as shown in Fig. 2.

Heat transfer in the chiller evaporator is modelled by the following balance equation

$$M_e c_h \frac{dT_e}{d\tau} = \dot{m}_e c_h \left(T_{23} - T_{21}\right) - \dot{Q}_e \left(\tau, T_e, T_c\right) \,, \tag{23}$$

where

$$T_e = \frac{T_{23} + T_{21}}{2} \,, \tag{24}$$

and T_{23} – evaporator inlet temperature, T_{21} – evaporator outlet temperature (and cooling receiver inlet temperature), $\dot{Q}_e$ – cooling capacity characteristics.

Heat balance in the mixing valve on the cold side (γ in Fig. 2) may be written as

$$\dot{m}_h c_h \left[T_{23}(\tau) - T_{22}(\tau)\right] = \dot{m}_b c_h \left[T_{21}(\tau) - T_{23}(\tau)\right] \,. \tag{25}$$

Heat transfer in the chiller generator is described with a balance equation

$$M_g c_g \frac{dT_g}{d\tau} = \dot{m}_g c_g \left(T_{14} - T_{15}\right) - \dot{Q}_g \,, \tag{26}$$

where

$$T_g = \frac{T_{14} + T_{15}}{2} \,, \tag{27}$$

$\dot{Q}_g$ is evaluated from the chiller heat generator characteristics and the generator inlet and outlet temperatures are denoted by T_{14}, T_{15}, respectively.

Heat supplied from the district network (*2* in Fig. 2) is taken into account through the balance equations for the substation heat exchanger hot side

$$M_d c_d \frac{dT_d}{d\tau} = \dot{m}_d c_d \left(T_{01} - T_{02}\right) - \frac{T_d - T_{dg}}{R_{dg}} \,, \tag{28}$$

and cold side

$$M_{dg} c_g \frac{dT_{dg}}{d\tau} = \dot{m}_g c_g \left(T_{15} - T_{11}\right) + \frac{T_d - T_{dg}}{R_{dg}} \,, \tag{29}$$

where

$$T_d = \frac{T_{01} + T_{02}}{2} \,, \tag{30}$$

$$T_{dg} = \frac{T_{11} + T_{15}}{2} \,, \tag{31}$$

$$R_{cg} = \frac{1}{A_{cg}} \left(\frac{1}{\alpha_{cg}} + \frac{\delta_{wcg}}{\lambda_{wcg}} + \frac{\delta_c}{\lambda_c}\right) \,, \tag{32}$$

$$R_{dg} = \frac{1}{A_{dg}} \left(\frac{1}{\alpha_{dg}} + \frac{\delta_{wdg}}{\lambda_{wdg}} + \frac{1}{\alpha_d}\right) \,, \tag{33}$$

and T_{01} is district heating inlet temperature, T_{02} –outlet temperature at district network return, T_{11} – chiller generator outlet temperature, T_{15} – outlet temperature at substation heat exchanger cold side (see Fig. 2).

The hot water tank with a solar electric heater (*5* in Fig. 2) is modelled with the balance equation

$$M_v c_g \frac{dT_v}{d\tau} = \dot{m}_g c_g \left(T_{11} - T_{12}\right) + P_v - \dot{Q}_{va} \,, \tag{34}$$

where

$$T_v = \frac{T_{11} + T_{12}}{2} \,, \tag{35}$$

and $\dot{Q}_{va}$ represents heat losses in the tank.

Finally, the mixing valve *12* in Fig. 2 is taken into account by

$$\dot{m}_c c_g \left[T_{13} - T_{14} \right] = \left(\dot{m}_g - \dot{m}_c \right) c_g \left[T_{14} - T_{12} \right]. \tag{36}$$

The equations presented above make a closed set that was solved in Lab-VIEW Control Design and Simulation module using the adaptive Runge-Kutta method for unknown temperatures T_i, T_h, T_w, T_p, T_f, T_u, T_c, T_{cg}, T_e, T_g, T_{dg} and T_v. The set of model equations may be transformed into a normal form that is convenient for numerical integration as shown in the Appendix.

4   Calculation results

It has been assumed that the cooling system will maintain the temperature $T_{iset} = 25°C$ in the rooms and will operate from 7 a.m. to 4 p.m. During this time, the adsorption chiller will be running. The first proportional-integral controller that controls the three-way valve *7* (Fig. 2) is designed to maintain the temperature in the room at the preset level T_{iset}. The second proportional-integral controller will control the process of thermal storage charging and discharging. This will be accomplished by varying the flow rate of fluid flowing through the bypass using three-way valve *12* (Fig. 2). For the purpose of the present calculations, however, it was assumed that a simpler procedure would be used. During the period when the AC system is off, the storage will be cut off. During the period of AC operation, there will be a flow through the LHTES1 storage with a rate of $\dot{m}_g$. The calculations were performed for input data on T_{01}, T_a and $\dot{m}$ obtained for the thermal node of the office building of the Ostrołęka Thermal Power Station. In addition, the heat load data $\dot{Q}_s$ were calculated in an external procedure and loaded before the calculations started. These data had a time resolution of 15 min. It was assumed that the heat storage was precharged to 64°C, corresponding to the initial temperature T_{01} of the water supplying the heat substation. To avoid numerical instability at the beginning of the calculation, the remaining initial temperatures of the elements in the heating circuit were also assumed to be 64°C. The initial temperature of the elements in the cooling circuit was 21°C. The calculation also assumed that the average temperature in the recooling circuit is 4°C higher than the air temperature T_a. This value is in accordance with the dry cooler selection sheet.

The calculations were carried out for two cases, namely for a system without a heat storage and for a storage containing 1000 kg of RT62HC

material. The evolution of the modelled indoor temperature in the office is shown in Fig. 17 for both cases.
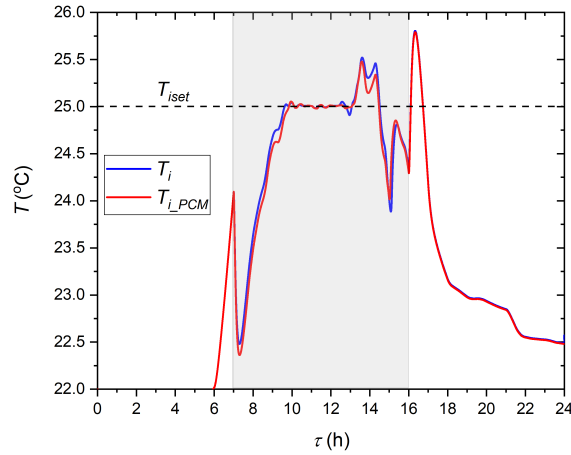

Figure 17: Evolution of the calculated temperature inside the office with (T_{i_PCM}) and without (T_i) LHTES. The shaded area indicates the period when the air conditioning system was on.

Temperatures of other components modelled in the office are shown in Fig. 18. Figure 19 presents the evolution of average temperatures in the main elements of the heating circuit. During the occupied period, T_i is
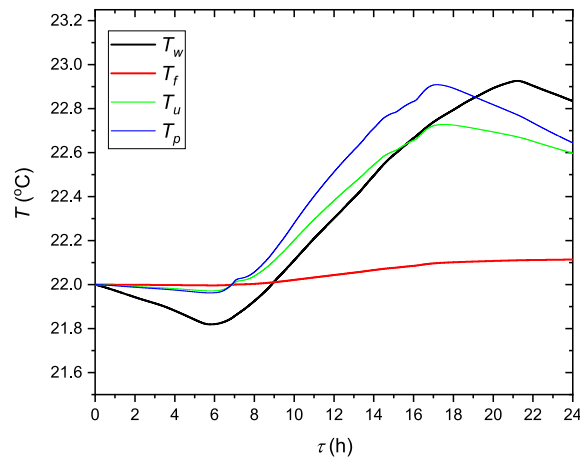
Figure 18: Variation of the temperatures T_w, T_f, T_u, T_p in the modelled office (case with PCM storage).

stabilized in the comfort zone by the cooling system. Building elements also stabilize the temperature, making its changes slower (Fig. 18). It can be seen (Fig. 17) that the T_i is below the set temperature from 7 a.m. to about 10 a.m., the reason being that the $\dot{Q}_e$ is higher than needed as the control of the valve *12* (Fig. 2) was not implemented in the model. For this reason, also the temperature T_{i_PCM}) did not change significantly (Fig. 17) for the case when PCM storage supports the chiller. It is anticipated that T_{i_PCM} profile will improve when a control algorithm for the process of proper charging and discharging of LHTES will be included in future model studies. It should also be noted that the use of the storage allowed us to raise the supply temperature of the adsorption chiller by 4°C, which translates into a 2.8% increase in cooling capacity.
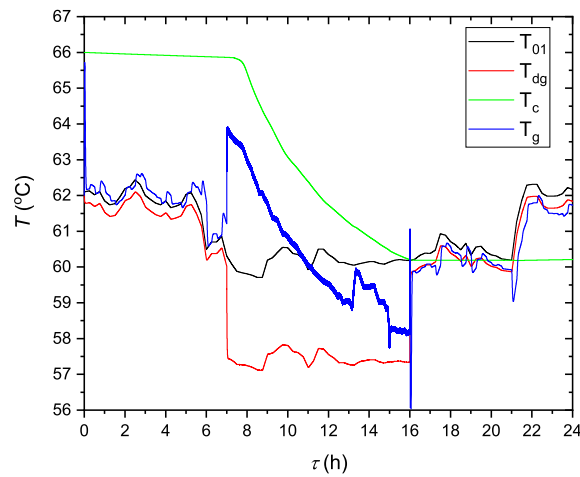
Figure 19: Evolution of the inlet HTF temperature T_{01} and main temperatures T_{dg}, T_c, T_g in the heating circuit.

5   Conclusions

The paper presents the analysis of an air conditioning system based on the adsorption chiller driven by district heat and supported by phase change material storage. The storage is aimed at optimization of the adsorption chiller performance. The operation of the complete system is described mathematically by the lumped parameter model. Example calculations were performed for cooling the office building in Ostrołęka (Poland). Preliminary analysis of climate conditions at the system location, the building

cooling demand and historic data on district hot water supply allowed us to determine the working parameters of the chiller unit and led to a conclusion that its efficient operation will require support with the heat accumulated in the PCM storage. Based on numerical simulations of the system operation during an exceptionally hot summer day (see Figs. 7–9), the RT62HC was selected as a suitable PCM for the latent heat storage.

Preliminary simulations showed that the storage with the selected PCM allows us to improve the performance of the adsorption chiller in the analyzed system. It should be noted that the target operation of the storage is to support the main system during the peak cooling demand. For this reason, the selected temperature profile for July 22, 2020 does not correspond to the design assumptions.

The model presented here is a valuable tool for assessing the range of temperatures in the research of a system planned for implementation. In addition, it allows us to test control algorithms for the entire system and, in particular, the process of charging and discharging the storage. Experimental work is planned in the near future that will allow for further development and validation of the model equations and boundary conditions.

Acknowledgements

References

[1] Leśko M., Bujalski W., Futyma K.: *Operational optimization in district heating systems with the use of thermal energy storage.* Energy **165**(2018), 902–15. doi: 10.1016/j.energy.2018.09.141

[2] Badyda K., Bujalski W., Niewiński G., Warchoł M.: *Selected issues related to heat storage tank modelling and optimisation aimed at forecasting its operation.* Arch. Thermodyn. **32**(2011), 3, 3–31. doi: 10.2478/v10173-011-0010-8

[3] Marini D., Buswell R.A., Hopfe C.J.: *Development of a dynamic analytical model for estimating waste heat from domestic hot water systems.* Energy Build. **247**(2021), 111119. doi: 10.1016/j.enbuild.2021.111119

[4] Khoury S., Maatouk C., Khoury K.. El Khatounian F.: *Optimization methodology of thermal energy storage systems for domestic water heating applications with different configurations.* J. Energy Stor. **50**(2022), 104530. doi: 10.1016/j.est.2022.104530

[5] Energy Regulatory Office: Thermal power industry in numbers – 2016 (A. Buńczyk, Ed.). URE, Warszawa 2017 (in Polish).

[6] Energy Regulatory Office: Thermal power industry in numbers – 2021. URE, Warszawa 2022 (in Polish). – Energetyka cieplna w liczbach 2020. Warszawa 2022.

[7] Poland – Country Commercial Guide 2022. https://www.trade.gov/country-commercial-guides/poland-energy-sector

[8] Energy consumption in households in 2018 (K. Walkowska, Ed.). GUS, Warszawa 2019. https://stat.gov.pl/publikacje/

[9] Lesko M., Bujalski W.: *Modeling of district heating networks for the purpose of operational optimization with thermal energy storage.* Arch. Thermodyn. **38**(2017), 4, 139–163. doi: 10.1515/aoter-2017-0029

[10] Milewski J., Szabłowski Ł., Bujalski W.: *Identification of the objective function for optimization of a seasonal thermal energy storage system.* Arch. Thermodyn. **35**(2014), 4, 69–81. doi: 10.2478/aoter-2014-0034

[11] Guelpa E., Verda V.: *Thermal energy storage in district heating and cooling systems: A review.* Appl. Energ. **252** (2019),113474. doi: 10.1016/j.apenergy.2019.113474

[12] Al-Yasiri Q., Szabó M., Arici M.: *A review on solar-powered cooling and air-conditioning systems for building applications.* Energy Rep. **8** (2022), 2888–2907. doi: 10.1016/j.egyr.2022.01.172

[13] Kuczyńska A., Szaflik W.: *Absorption and adsorption chillers applied to air conditioning systems.* Arch. Thermodyn. **31**(2010), 2, 77–94. doi: 10.2478/v10173-010- 0010-0

[14] Grzebielec A., Rusowicz A.: *Analysis of the use of adsorption processes in trigeneration systems.* Arch. Thermodyn. **34**(2013), 4, 35–49. doi: 10.2478/aoter-2013-0028

[15] Amiri Rad E., Davoodi V.: *Thermo-economic evaluation of a hybrid solar-gas driven and air-cooled absorption chiller integrated with hot water production by a transient modeling.* Renew. Energ. **163** (2021), 1253–64. doi: 10.1016/j.renene.2020.08.157

[16] Rouf R.A., Jahan N., Alam K.C.A., Sultan A.A., Saha B.B., Saha S.C.: *Improved cooling capacity of a solar heat driven adsorption chiller.* Case Stud. Therm. Eng. **17** (2020), 100568. doi: 10.1016/j.csite.2019.100568

[17] Naseem M., Park S., Lee S.: *Experimental and theoretical analysis of a trigeneration system consisting of adsorption chiller and high temperature PEMFC.* Energ, Convers, Manage. **251** (2022), 114977. doi: 10.1016/j.enconman.2021.114977

[18] Karwacki J., Kwidziński R.: Theoretical analysis of a latent thermal energy storage system with an adsorption chiller. Polska Energetyka Słoneczna (2016), 1-4, 59–64.

[19] Karwacki J., Kwidziński R., Lackowski M., Kapica P., Śniadał T., Le-
     puta P., Laskowski M.: *Analysis of the use of heat storage with PCM material
     in the case of a mismatch in the productivity of the source and receiver of cooling.*
     Nowa Energia **67**(2019), 2, 40–9 (in Polish).

[20] Szczęśniak A., Bujalski W., Grzebielec A., Futyma K., Karwacki J., Rol-
     ka P.: *A hybrid district heating substation with an adsorption chiller and PCM
     storage units: a concept and preliminary study.* E3S Web Conf. **321**(2021), 02009.
     doi: 10.1051/e3sconf/202132102009

[21] Gjoka K., Rismanchi B., Crawford R.H.: *Fifth-generation district heating and
     cooling systems: A review of recent advancements and implementation barriers.* Re-
     new. Sust. Energ. Rev. **171**(2023), 112997. doi: 10.1016/j.rser.2022.112997

[22] Buffa S., Cozzini M., D'Antoni M., Baratieri M., Fedrizzi R.: *5th generation district
     heating and cooling systems: A review of existing cases in Europe.* Renew. Sust.
     Energ. Rev. **104** (2019), 504–22. doi: 10.1016/j.rser.2018.12.059

[23] Wang X., Li W., Luo Z., Wang K., Shah S.P.: *A critical review on phase change
     materials (PCM) for sustainable and energy efficient building: Design, characteris-
     tic, performance and application.* Energ. Buildings **260**(2022), 111923. doi: 10.1016/
     j.enbuild.2022.111923

[24] Souayfane F., Fardoun F., Biwole P.H.: *Phase change materials (PCM) for
     cooling applications in buildings: A review.* Energy Buildings **129** (2016), 396–431.
     doi: 10.1016/j.enbuild.2016.04.006

[25] Koželj R., Osterman E., Leonforte F., Del Pero C., Miglioli A., Zavrl E.,
     Stropnik R., Aste N., Stritih U.: *Phase-change materials in hydronic heating
     and cooling systems: A literature review.* Materials **13**(2020), 2971. doi: 10.3390/
     ma13132971

[26] Mehling H., Cabeza L.F.: *Heat and cold storage with PCM. An up to date intro-
     duction into basics and applications.* Springer, Berlin 2008. doi: 10.1007/978-3-540-
     68557-9

[27] Dubovsky V., Ziskind G., Letan R.: *Temperature moderation in a multistorey
     building by melting of a phase-change material.* Arch. Thermodyn. **34**(2013), 1,
     85–101. doi: 10.2478/aoter-2013-0006

[28] Jaworski M.: *Thermal performance of building element containing phase change
     material (PCM) integrated with ventilation system – An experimental study.* Appl.
     Therm. Eng. **70**(2014), 665–74. doi: 10.1016/j.applthermaleng.2014.05.093

[29] Khan M.M.A., Saidur R., Al-Sulaiman F.A.: *A review for phase change ma-
     terials (PCMs) in solar absorption refrigeration systems.* Renew. Sust. Energ. Rev.
     76 (2017), 105–37. doi: 10.1016/j.rser.2017.03.070

[30] Almasri R.A., Abu-Hamdeh N.H., Esmaeil K.K., Suyambazhahan S.: *Thermal
     solar sorption cooling systems, a review of principle, technology, and applications.*
     Alexandria Eng. J. **61** (2022), 367–402. doi: 10.1016/j.aej.2021.06.005

[31] Chauhan P.R., Kaushik S.C., Tyagi S.K.: *Current status and technological ad-
     vancements in adsorption refrigeration systems: A review.* Renew. Sust. Energ. Rev.
     154(2022), 111808. doi: 10.1016/j.rser.2021.111808

[32] Hassan A.A., Elwardany A.E., Ookawara S., Ahmed M., El-Sharkawy I.I.: *Integrated adsorption-based multigeneration systems: A critical review and future trends.* Int. J. Refrig. **116**(2020), 129–45. doi: 10.1016/j.ijrefrig.2020.04.001

[33] Ullah K.R., Saidur R., Ping H.W., Akikur R.K., Shuvo N.H.: *A review of solar thermal refrigeration and cooling methods.* Renew. Sust. Energ. Rev. **24**(2013), 499–513. doi: 10.1016/j.rser.2013.03.024

[34] Varvagiannis E., Charalampidis A., Zsembinszki G., Karellas S., Cabeza L.F.: *Energy assessment based on semi-dynamic modelling of a photovoltaic driven vapour compression chiller using phase change materials for cold energy storage.* Renew. Energ. **163** (2021), 198–212. doi: 10.1016/j.renene.2020.08.034

[35] Ghorbani B., Kowsary F., Ebrahimi S., Vijayaraghavan K.: *CFD modeling and optimization of a latent heat storage unit for running a solar assisted single effect Li-Br absorption chiller using multi-objective genetic algorithm.* Sustain Cities Soc. **34**(2017), 321–34. doi: 10.1016/j.scs.2017.05.023

[36] Raj V.K., Baiju V., Junaid F.P.: *Numerical investigations of thermal performance enhancement in phase change energy storage system effective for solar adsorption cooling systems.* J. Energ. Stor. **45** (2022), 103696. doi: 10.1016/j.est.2021.103696

[37] Karwacki J.: *Cooling system with PCM storage for an office building: Experimental investigation aided by a model of the office thermal dynamics.* Materials **14**(2021), 6, 1356. doi: 10.3390/ma14061356

[38] Ochrymiuk T.: *Numerical analysis of microholes film/effusion cooling effectiveness.* J. Therm. Sci. **26** (2017), 459–464. doi: 10.1007/s11630-017-0962-3

[39] Szwaba R., Ochrymiuk T., Lewandowski T., Czerwinska J.: *Experimental investigation of microscale effects in perforated plate aerodynamics.* ASME J. Fluids Eng. **135**(2013), 12, 1–10. doi: 10.1115/1.4024962

[40] Ochrymiuk T.: *Numerical prediction of film cooling effectiveness over flat plate using variable turbulent Prandtl number closures.* J. Therm. Sci. **25**(2016), 280–286. doi: 10.1007/s11630-016-0861-z

[41] Kurowski M., Szwaba R., Telega J., Flaszynski P., Tejero F., Doerffer P.: *Wall distance effect on heat transfer at high flow velocity.* Aircr. Eng. Aerosp. Technol. **91**(2019), 9, 1180–1186. doi: 10.1108/AEAT-01-2018-0022

[42] Szwaba R., Kaczynski P., Telega J., Doerffer P.: *Influence of internal channel geometry of gas turbine blade on flow structure and heat transfer.* J. Therm. Sci. **26**(2017), 514–522. doi: 10.1007/s11630-017-0968-x

[43] Telega J., Szwaba R., Śmiałek M.A.: *Compressible gas density measurement by means of Fourier analysis of interferograms.* Measurement **189**(2022), 110458. doi: 10.1016/j.measurement.2021.110458

[44] Fahrenheit GmbH. https://fahrenheit.cool/en/

[45] Cabeza L.F., Barreneche C., Martorell I., Miró L., Sari-Bey S., Fois M., *et al.*: *Unconventional experimental technologies available for phase change materials (PCM) characterization. Part 1. Thermophysical properties.* Renew. Sust. Energ. Rev. **43**(2015), 1399–1414. doi: 10.1016/j.rser.2014.07.191

[46] ROLKA P., PRZYBYLINSKI T., KWIDZINSKI R., LACKOWSKI M.: *The heat capacity of low-temperature phase change materials (PCM) applied in thermal energy storage systems.* Renew. Energ. **172**(2021), 541–550. doi: 10.1016/j.renene.2021.03.038

[47] ROLKA P., KWIDZINSKI R., PRZYBYLINSKI T., TOMASZEWSKI A.: *Thermal characterization of medium-temperature phase change materials (PCMS) for thermal energy storage using the T-history method.* Materials **14**(2021), 7371. doi: 10.3390/ma14237371

[48] KARWACKI J., KWIDZIŃSKI R.: *Experimental investigation of PCM thermal energy storage charge and discharge process with aperiodic (ramp) temperature inputs.* E3S Web Conf. **70**(2018), 03005. doi: 10.1051/e3sconf/20187003005

[49] PCM Axiotherm ATP60 Data sheet. https://www.axiotherm.de/en/download/project/productdatasheet/file/20/

[50] PCM Axiotherm ATP70 Data sheet. https://www.axiotherm.de/en/download/project/productdatasheet/file/21/

[51] PCM Croda Therm 60 Data sheet. https://www.crodaindustrialspecialties.com/en-gb/product-finder/product/1803-crodatherm_1_60

[52] PCM Rubitherm RT62HC Data sheet. https://www.rubitherm.eu/media/products/datasheets/Techdata_-RT62HC_EN_09102020.PDF

[53] PCM Rubitherm RT69HT Data sheet. https://www.rubitherm.eu/media/products/datasheets/Techdata_-RT69HC_EN_09102020.PDF

[54] PCM Rubitherm RT70HC Data sheet. https://www.rubitherm.eu/media/products/datasheets/Techdata_-RT70HC_EN_09102020.PDF

[55] MATYSKO R., DYCZKOWSKA M.: *Thermal dynamics of a building.* Trans. Inst. Fluid-Flow Mach. **141**(2018), 31–40.

Appendix

The set of model Eqs. (3)–(9), (20)–(31), (34)–(36) is a mix of differential and algebraic equations. To facilitate numerical integration, it has been transformed into the set of differential equations in the normal form (i.e. solved with respect to the differentials).

In the first step, the inlet/outlet temperatures should be eliminated from the differential equations. This is done by substitution of the solutions of two algebraic sets of equations. Namely, solving the set of Eqs. (22), (27), (31), (35), (36) with the following definition for the 3-way valve setting:

$$x_1 = \frac{\dot{m}_c}{\dot{m}_g}\,, \tag{A.1}$$

one gets

$$T_{11} = 2T_v - T_{cg} + \frac{T_g + T_v - T_{cg} - T_{dg}}{x_1 - 1} \,, \tag{A.2}$$

$$T_{12} = 2T_v - T_{11} = T_{cg} - \frac{T_g + T_v - T_{cg} - T_{dg}}{x_1 - 1} \,, \tag{A.3}$$

$$T_{13} = T_{cg} + \frac{T_g + T_v - T_{cg} - T_{dg}}{x_1 - 1} \,, \tag{A.4}$$

$$T_{14} = 2\left(T_g + T_v - T_{dg}\right) - T_{cg} + \frac{T_g + T_v - T_{cg} - T_{dg}}{x_1 - 1}$$
$$= 2\left(T_g + T_v - T_{dg}\right) - T_{12} \,, \tag{A.5}$$

$$T_{15} = 2T_{dg} - T_{11} = 2\left(T_{dg} - T_v\right) + T_{cg} - \frac{T_g + T_v - T_{cg} - T_{dg}}{x_1 - 1}$$
$$= 2\left(T_{dg} - T_v\right) + T_{12} \,. \tag{A.6}$$

Additionally, from Eq. (30) it follows that

$$T_{02} = 2T_d - T_{01} \,. \tag{A.7}$$

Similarly, with the definition

$$x_2 = \frac{\dot{m}_h}{\dot{m}_e} \,, \tag{A.8}$$

the set of Eqs. (5), (24), (25) is solved for temperatures in the cooling loop:

$$T_{21} = T_h - \frac{T_e - T_h}{x_2 - 1} \,, \tag{A.9}$$

$$T_{22} = 2T_h - T_{21} = T_h + \frac{T_e - T_h}{x_2 - 1} \,, \tag{A.10}$$

$$T_{23} = 2T_e - T_{21} = 2T_e - T_h + \frac{T_e - T_h}{x_2 - 1} \,. \tag{A.11}$$

The above expressions for T_{02}, T_{11}, T_{12}, T_{13}, T_{14}, T_{15}, T_{21}, T_{22}, and T_{23} are substituted into Eqs. (4), (21), (23), (26), (28), (29), (34). After simplification, the model equations in normal form can be written as follows:

indoor air

$$\frac{dT_i}{d\tau} = \beta_{i1}\left(T_h - T_i\right) + \beta_{i2}\left(T_w - T_i\right) + \beta_{i3}\left(T_p - T_i\right) + \beta_{i4}\left(T_f - T_i\right)$$
$$+ \; \beta_{i5}\left(T_u - T_i\right) + \beta_{i6}\left(T_a - T_i\right) + \beta_{i7}\dot{Q}_s \,, \tag{A.12}$$

HTF in air cooler

$$\frac{dT_h}{d\tau} = \beta_{h1}\frac{x_2}{1-x_2}\left(T_e - T_h\right) + \beta_{h2}\left(T_i - T_h\right), \qquad \text{(A.13)}$$

outer wall

$$\frac{dT_w}{d\tau} = \beta_{w1}\left(T_i - T_w\right) + \beta_{w2}\left(T_a - T_w\right), \qquad \text{(A.14)}$$

inner wall

$$\frac{dT_p}{d\tau} = \beta_{p1}\left(T_i - T_p\right) + \beta_{p2}\left(T_{pb} - T_p\right), \qquad \text{(A.15)}$$

floor

$$\frac{dT_f}{d\tau} = \beta_{f1}\left(T_i - T_f\right) + \beta_{f2}\left(T_{fa} - T_f\right), \qquad \text{(A.16)}$$

ceiling

$$\frac{dT_u}{d\tau} = \beta_{u1}\left(T_i - T_u\right) + \beta_{u2}\left(T_{ua} - T_u\right), \qquad \text{(A.17)}$$

PCM in LHTES3

$$\frac{dT_c}{d\tau} = \beta_{c1}\frac{T_{cg} - T_c}{c_c\left(T_c\right)} + \beta_{c2}\frac{\dot{Q}_{ca}}{c_c\left(T_c\right)}, \qquad \text{(A.18)}$$

HTF in LHTES3

$$\frac{dT_{cg}}{d\tau} = \beta_{cg1}\frac{x_1}{x_1-1}\left(T_{cg} + T_{dg} - T_g - T_v\right) + \beta_{cg2}\left(T_c - T_{cg}\right), \qquad \text{(A.19)}$$

adsorption chiller evaporator

$$\frac{dT_e}{d\tau} = \beta_{e1}\frac{x_2}{1-x_2}\left(T_h - T_e\right) - \beta_{e2}\dot{Q}_e\left(\tau, T_e, T_c\right), \qquad \text{(A.20)}$$

adsorption chiller heat generator

$$\frac{dT_g}{d\tau} = \beta_{g1}\left[\frac{x_1}{x_1-1}\left(T_g + 2T_v - T_{cg} - 2T_{dg}\right) + \frac{1}{x_1-1}\left(T_{dg} - T_v\right)\right]$$
$$+ \ \beta_{g2}\dot{Q}_g\,, \qquad \text{(A.21)}$$

district heating exchanger cold side

$$\frac{dT_{dg}}{d\tau} = \beta_{dg1}\left[\frac{x_1}{x_1-1}\left(T_{cg} + T_{dg} - 2T_v\right) + \frac{1}{x_1-1}\left(T_v - T_g\right)\right]$$
$$+ \beta_{dg2}\left(T_d - T_{dg}\right), \qquad \text{(A.22)}$$

district heating exchanger hot side

$$\frac{dT_d}{d\tau} = \beta_{d1} \left(T_{01} - T_d \right) + \beta_{d2} \left(T_{dg} - T_d \right),$$ (A.23)

hot water tank

$$\frac{dT_v}{d\tau} = \beta_{v1} \left[\frac{x_1}{x_1 - 1} \left(T_v - T_{cg} \right) + \frac{1}{x_1 - 1} \left(T_g - T_{dg} \right) \right]$$
$$+ \ \beta_{v2} \left(P_v - \dot{Q}_{va} \right).$$ (A.24)

The coefficients β in the above equations are constants defined by

$$\beta_{i1} = \frac{1}{M_i c_i R_h},$$ (A.25)

$$\beta_{i2} = \frac{1}{M_i c_i R_{wi}},$$ (A.26)

$$\beta_{i3} = \frac{1}{M_i c_i R_{pi}},$$ (A.27)

$$\beta_{i4} = \frac{1}{M_i c_i R_{fi}},$$ (A.28)

$$\beta_{i5} = \frac{1}{M_i c_i R_{ui}},$$ (A.29)

$$\beta_{i6} = \frac{1}{M_i c_i R_o},$$ (A.30)

$$\beta_{i7} = \frac{1}{M_i c_i},$$ (A.31)

$$\beta_{h1} = \frac{2\dot{m}_e}{M_h},$$ (A.32)

$$\beta_{h2} = \frac{1}{M_h c_h R_h},$$ (A.33)

$$\beta_{w1} = \frac{1}{M_w c_w R_{wi}},$$ (A.34)

$$\beta_{w2} = \frac{1}{M_w c_w R_{wa}},$$ (A.35)

$$\beta_{p1} = \frac{1}{M_p c_p R_{pi}},$$ (A.36)

$$\beta_{p2} = \frac{1}{M_p c_p R_{pa}}\,, \tag{A.37}$$

$$\beta_{f1} = \frac{1}{M_f c_f R_{fi}}\,, \tag{A.38}$$

$$\beta_{f2} = \frac{1}{M_f c_f R_{fa}}\,, \tag{A.39}$$

$$\beta_{u1} = \frac{1}{M_u c_u R_{ui}}\,, \tag{A.40}$$

$$\beta_{u2} = \frac{1}{M_u c_u R_{ua}}\,, \tag{A.41}$$

$$\beta_{e1} = \frac{2\dot{m}_e}{M_e}\,, \tag{A.42}$$

$$\beta_{e2} = \frac{1}{M_e c_h}\,, \tag{A.43}$$

$$\beta_{c1} = \frac{1}{M_c R_{cg}}\,, \tag{A.44}$$

$$\beta_{c2} = \frac{-1}{M_c}\,, \tag{A.45}$$

$$\beta_{cg1} = \frac{2\dot{m}_g}{M_{cg}}\,, \tag{A.46}$$

$$\beta_{cg2} = \frac{1}{M_{cg} c_g R_{cg}}\,, \tag{A.47}$$

$$\beta_{g1} = \frac{2\dot{m}_g}{M_g}\,, \tag{A.48}$$

$$\beta_{g2} = \frac{-1}{M_g c_g}\,, \tag{A.49}$$

$$\beta_{dg1} = \frac{2\dot{m}_g}{M_{dg}}\,, \tag{A.50}$$

$$\beta_{dg2} = \frac{1}{M_{dg} c_g R_{dg}}\,, \tag{A.51}$$

$$\beta_{d1} = \frac{2\dot{m}_d}{M_d}\,, \tag{A.52}$$

$$\beta_{d2} = \frac{1}{M_d c_d R_{dg}}\,, \tag{A.53}$$

$$\beta_{v1} = \frac{2\dot{m}_g}{M_v} \,, \tag{A.54}$$

$$\beta_{v2} = \frac{1}{M_v c_g} \,. \tag{A.55}$$

The set of ordinary differential equations (A.12)–(A.24) with coefficients (A.25)–(A.50) can be solved for the unknown average temperatures T_i, T_w, T_p, T_f, T_u, T_c, T_{cg}, T_e, T_g, T_{dg}, T_d, and T_v, provided that temporal changes of x_1, x_2, $\dot{Q}_s$, $\dot{Q}_{ca}$, $\dot{Q}_e$, $\dot{Q}_g$, $\dot{Q}_{va}$, P_v, and T_{01} are defined by auxiliary functions. Afterwards, the distributions of temperatures (A.2)–(A.7), (A.9)–(A.11) can also be reconstructed.